



# Insight into the acceleration in oxidation kinetics ahead of stress corrosion crack of alloy 690 in simulated PWR primary water



Wenjun Kuang<sup>a,\*</sup>, Miao Song<sup>b</sup>, Xingyu Feng<sup>a</sup>

<sup>a</sup> Center for Advancing Materials Performance from the Nanoscale (CAMP-Nano), State Key Laboratory for Mechanical Behavior of Materials, Xi'an Jiaotong University, Xi'an 710049, PR China

<sup>b</sup> Department of Nuclear Engineering and Radiological Sciences, University of Michigan, Ann Arbor, MI 48109, USA

## ARTICLE INFO

### Keywords:

Alloy  
STEM  
Oxidation  
Interfaces  
Kinetic parameters  
Stress corrosion

## ABSTRACT

The acceleration in oxidation kinetics beyond a stress corrosion crack of alloy 690 in simulated PWR primary water was clarified by comparing the oxide depths at two identical carbide/matrix interfaces along a single grain boundary. Compact chromia layer formed along these two interfaces at vastly different rates. Stress concentration ahead of the crack tip only slightly increased the oxidation rate as the crack is still very shallow. Deformation localization near the crack plays a dominant role in accelerating oxidation kinetics as the associated high vacancy concentration can promote the diffusivity of oxygen by over an order of magnitude.

## 1. Introduction

Stress corrosion cracking (SCC) is an important mode of environment assisted degradation of structure material in light water nuclear power plant. For example, the SCC of stainless steels (used in piping and core internal components) and nickel base alloys (used as heat exchanger tube in the steam generator of pressurized water reactor (PWR)) has been baffling the nuclear industry for decades [1–3] and attracted extensive research attention. Now abundant experiment results indicate that preferential intergranular oxidation is an inevitable precursor for SCC to initiate and propagate in Fe-Cr-Ni alloys like alloy 600. Selective internal oxidation (SIO) has long been proposed to explain the intergranular SCC (IGSCC) initiation of alloy 600 in PWR primary water [4–8]. According to this model, the grain boundary is embrittled by intergranular oxidation and crack initiates when the grain boundary strength falls below the external applied stress, as evidenced by some miniature mechanical tests on grain boundaries extracted from the pre-oxidized sample [9–12]. Compared to alloy 600, alloy 690 has higher SCC resistance due to its ability to form a Cr-rich protective oxide layer over the random high angle boundary which prevents the ingress of oxygen [13–15]. Nevertheless, this alloy is still susceptible to intergranular oxidation and then SCC initiation after the surface oxide layer is breached during dynamic straining [16,17]. Intergranular oxidation has also been unanimously observed ahead of SCC crack tips in a wide range of Fe-Cr-Ni alloys tested in high temperature water, such as austenitic stainless steel [18–21], alloy 600

[22–26] and alloy 690 [17,27,28] as well. Thus, intergranular oxidation is a vital precursor in the SCC process of the Fe-Cr-Ni alloys in light water nuclear power plant.

Although the mechanistic understanding of SCC of Fe-Cr-Ni alloys in high temperature water has been greatly improved thanks to the availability of modern analytical instruments, modeling the SCC process is still challenging partly due to the unclarified synergetic effects of the sub processes. Given that intergranular oxidation is an inevitable precursor in SCC, the growth rate of SCC should be directly related to the kinetics of intergranular oxide formation ahead of the crack tip. However, a critical issue in this theory is that the diffusivity of oxygen extrapolated from the classical high temperature diffusion data seems too low to explain the measured SCC propagation rate [4,29]. The diffusion rate of oxygen or other reactants near the crack tip should be accelerated significantly, and several mechanistic hypotheses have been proposed. Simonen et al. [30] predicted that nonequilibrium vacancy injection during corrosion could highly promote the solid-state diffusion of both substitutional solute and interstitial oxygen. Lozano-Perez et al. [26,31] proposed that the diffusion near the crack tip could be enhanced by the deformation-induced defects (like dislocation and deformation band) and stress concentration. Sennour et al. [23] and Guerre et al. [32] suggested that the SCC crack propagation of alloy 600 is controlled by the diffusion of Cr from the bulk material to the crack tip which is promoted by the high density of defect ahead of the crack tip. Thus, either concentrated defects or stress or both should be responsible for the enhanced diffusion near the crack tip. However, those

\* Corresponding author.

E-mail address: [wjkuang66@gmail.com](mailto:wjkuang66@gmail.com) (W. Kuang).

<https://doi.org/10.1016/j.corsci.2020.108943>

Received 24 June 2020; Received in revised form 2 August 2020; Accepted 12 August 2020

Available online 14 August 2020

0010-938X/ © 2020 Elsevier Ltd. All rights reserved.

qualitative theories are still elusive and haven't been experimentally substantiated due to the difficulty in experiment design.

Intergranular oxidation ahead of crack tip has also been widely reported in the creep and fatigue of Ni base superalloys in oxidizing gaseous environment at higher temperatures (above 550 °C) [33–37]. In these cases, the acceleration in the growth rate of intergranular oxide was normally thought due to the stress and termed as stress accelerated grain boundary oxidation (SAGBO) [38]. Such a concept may apply to the SCC of Fe-Cr-Ni alloys in high temperature water since similar process occurs at the crack tip, as noticed by Lu et al. [20]. Evans and his colleagues [39,40] developed a quantitative SAGBO model based on the principle that the stress gradient along the oxide intrusion can increase the anion vacancy flux to the crack tip and thus promote the growth rate of oxide intrusion. Shoji et al. [41] incorporated such consideration into a formulation for predicting the SCC growth rate of Ni base alloys. However, in the model developed by Evans et al. [39,40], only the effect of stress on the concentration of oxygen vacancy was considered while the possible effect on oxygen diffusivity was not addressed. In addition, the accuracy of this model has not been directly verified by experiments.

In conclusion, the acceleration mechanism in the oxidation kinetics ahead of crack tip should be further clarified in order to improve the mechanistic understanding of SCC of Fe-Cr-Ni alloys in high temperature water and reliably predict the SCC growth rate. In this work, in order to single out and study the effects of stress concentration/localized deformation near a crack tip on oxidation kinetics, a special intergranular SCC crack from alloy 690 was carefully analyzed after constant extension rate tensile (CERT) test in simulated PWR primary water. This grain boundary contains two identical carbide/matrix interfaces and only one interface cracked while the other one was intact, so the possible effects of interface structure or macroscopic mechanical condition on the oxidation kinetics can be canceled when comparing between these two interfaces. This peculiar sample provides a highly desirable opportunity to clarify the acceleration mechanism in oxidation kinetics ahead of the crack tip.

## 2. Experimental

### 2.1. Material

The alloy 690 block (57.6 wt.% Ni, 32.7% Cr, 8.64% Fe, 0.25% Mn, 0.315% Al, 0.08% Si and 0.02% C) was hot rolled to 8 mm-thick sheet at around 1100 °C, then solution annealed at 1100 °C for 1 h, and at last thermally treated (TT) for 17 h at 700 °C. As in our previous work [42–44], the block was machined into round tensile bars measuring 20 mm in gauge length and 2 mm in diameter. The gauge surface was mechanically abraded up to 4000 grit and electropolished for 30 s at 30 V in a solution of 10% (volume fraction) perchloric acid in methanol at –30 °C. The sample was cleaned three times alternately with methanol and acetone immediately after electropolishing. The sample was examined in scanning electron microscope (SEM) and no preferential corrosion was observed along the carbide/matrix interfaces or the grain boundaries which are free of precipitates.

### 2.2. Apparatus and methodology

CERT test was conducted in 360 °C high purity water in a refreshed water loop system. The dissolved hydrogen concentration was controlled at 18 cm<sup>3</sup> (STP) H<sub>2</sub>/kg H<sub>2</sub>O. The same procedure used in a previous work [28] was applied: the sample was quickly loaded to just below the yield point at a rate of 1.24 × 10<sup>-5</sup>/s after the environment condition stabilized and then the strain rate was lowered to 5 × 10<sup>-8</sup>/s. Fig. 1 shows the stress-strain curve during the CERT test. Lots of serrations appear on the curve due to dynamic strain aging [43]. The tensile sample was uniformly strained to 7% plastic strain after a total test time of 502 h.

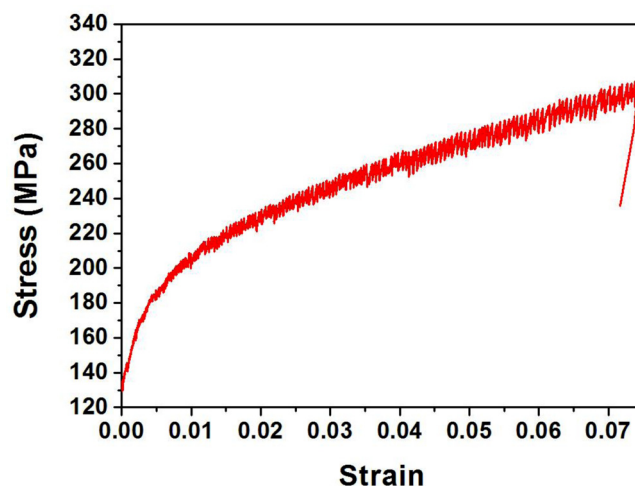


Fig. 1. Stress-strain curve of TT alloy 690 during constant extension rate tensile (CERT) test at 5 × 10<sup>-8</sup>/s in 360 °C high purity water containing 18 cm<sup>3</sup> (STP) H<sub>2</sub>/kg H<sub>2</sub>O.

The sampled grain boundary was first examined using scanning electron microscope (SEM) after the loading axis was aligned with the horizontal direction. Cross-section of the grain boundary was made using a focused ion beam (FIB) milling on an FEI Helios Nanolab according to the procedure described in a previous work [15]. The FIB sample was analyzed on a JEOL JEM-F200(HR) scanning transmission electron microscope (STEM) which is equipped with two 100 mm<sup>2</sup> energy dispersive spectroscopy (EDS) X-ray detectors and high angle annular dark-field (HAADF) detector. High resolution TEM images were taken using a JEOL 3100R05 and analyzed by Fast Fourier Transformation (FFT). Transmission Kikuchi diffraction (TKD) was performed on the FIB sample with an electron back-scattered diffraction (EBSD) detector attached to the Helios system at a working distance of 4.1 mm. The step size was set to 10 nm. The acceleration voltage was 30 kV and the beam current was 6.4 nA.

## 3. Results

Fig. 2a shows a SEM image of the sampled intergranular crack after the loading axis was aligned with the horizontal direction. A HAADF image of the cross section of grain boundary is presented in Fig. 2b. A continuous carbide layer was observed along the entire grain boundary. Thus, the grain boundary is composed of two carbide/matrix interfaces. Interestingly, one of the interfaces cracked while the other didn't. Penetrative internal oxide formed into the matrix from the sample surface (Fig. 2b), as reported in our previous work [45]. An enlarged image from the framed area in Fig. 2b is shown in Fig. 2c. There is a segment of compact oxide layer formed along both interfaces from the exposed end (Fig. 2c). The depths of oxide segments and the crack are denoted in Fig. 2c. The oxide was further analyzed through high resolution TEM imaging. Fig. 2d shows the high resolution TEM image of the oxide between carbide and matrix. FFT of the oxide/matrix interface indicates that the oxide has a hematite structure which probably corresponds to chromia. The oxide has specific orientation relationship with matrix: oxide < 100 > // matrix < 112 >, oxide {006} // matrix {111} (Fig. 2e). The preferential formation of chromia along the carbide/matrix interface has also been reported in alloy 600 and alloy 690 in previous work [46,47].

The structure of un-attacked interface was further characterized. Figs. 3a and 3b show the high resolution TEM image of the phase boundary between the left grain and carbide and the corresponding FFT. The FFT clearly indicates that the carbide is M<sub>23</sub>C<sub>6</sub> type and has a cube-on-cube orientation relationship with the grain (Fig. 3b) which has also been reported before [48,49]. The < 112 > zone axes are

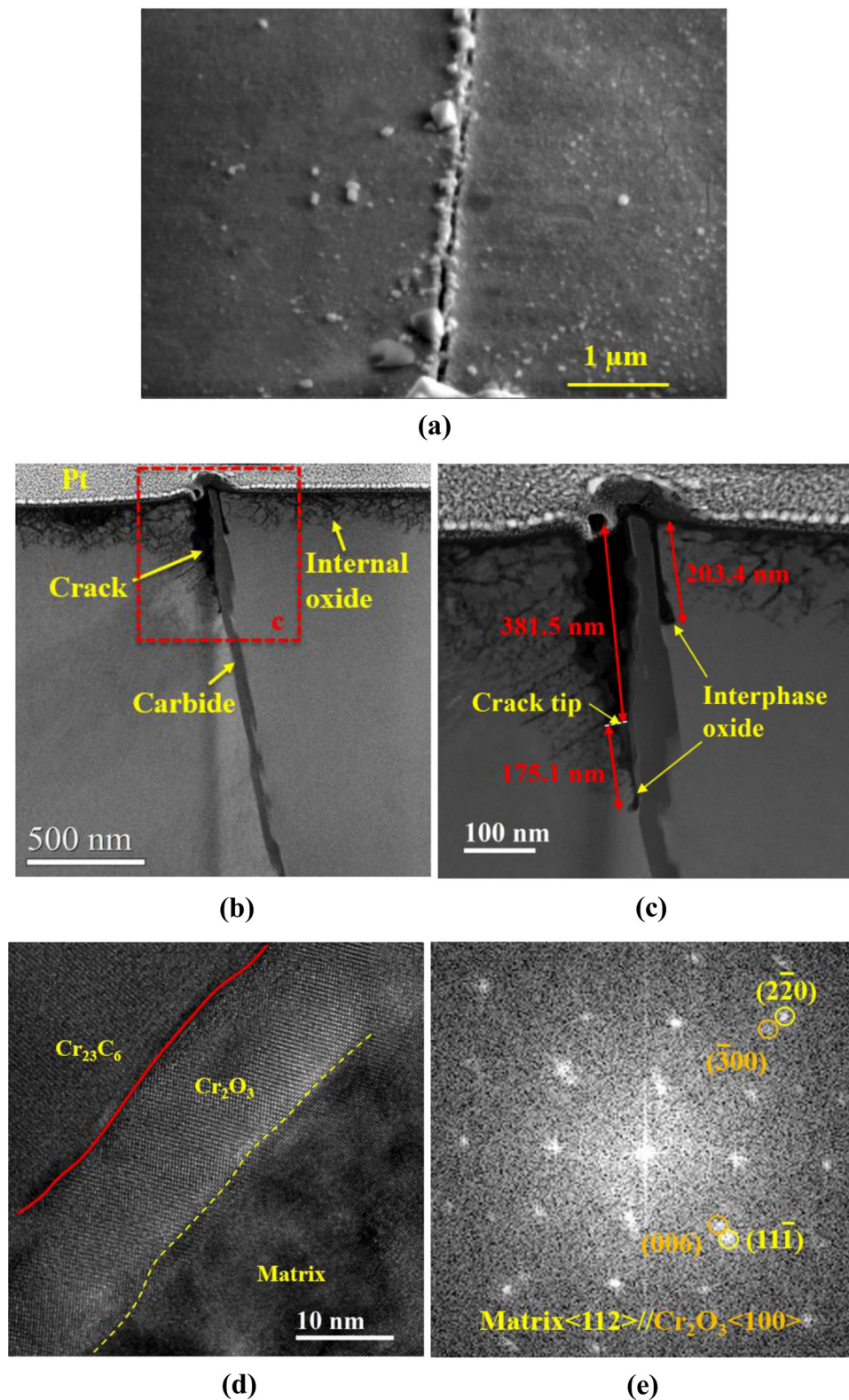


**Fig. 2.** (a) SEM image of the sampled intergranular crack, (b) HAADF image of the cross section of the grain boundary, (c) enlarged HAADF image of the framed area in (b), (d) high resolution TEM image of the interphase oxide and (e) FFT of the oxide.

perpendicular to the sample surface and the interface is aligned with the  $\{111\}$  plane. Interestingly, without changing orientation of the sample with respect to electron beam, the high resolution TEM image taken from the other phase boundary also shows cube-on-cube orientation relationship between the carbide and right grain (Figs. 3c and

3d). The  $\langle 112 \rangle$  zone axes are also perpendicular to the sample surface and the interface is aligned with the  $\{111\}$  plane. Fig. 3e shows that there is a boundary within the carbide. Thus, there are two layers of carbides along the  $\{111\}$  plane of matrix and the  $\langle 112 \rangle$  zone axes of these two carbide layers coincide.

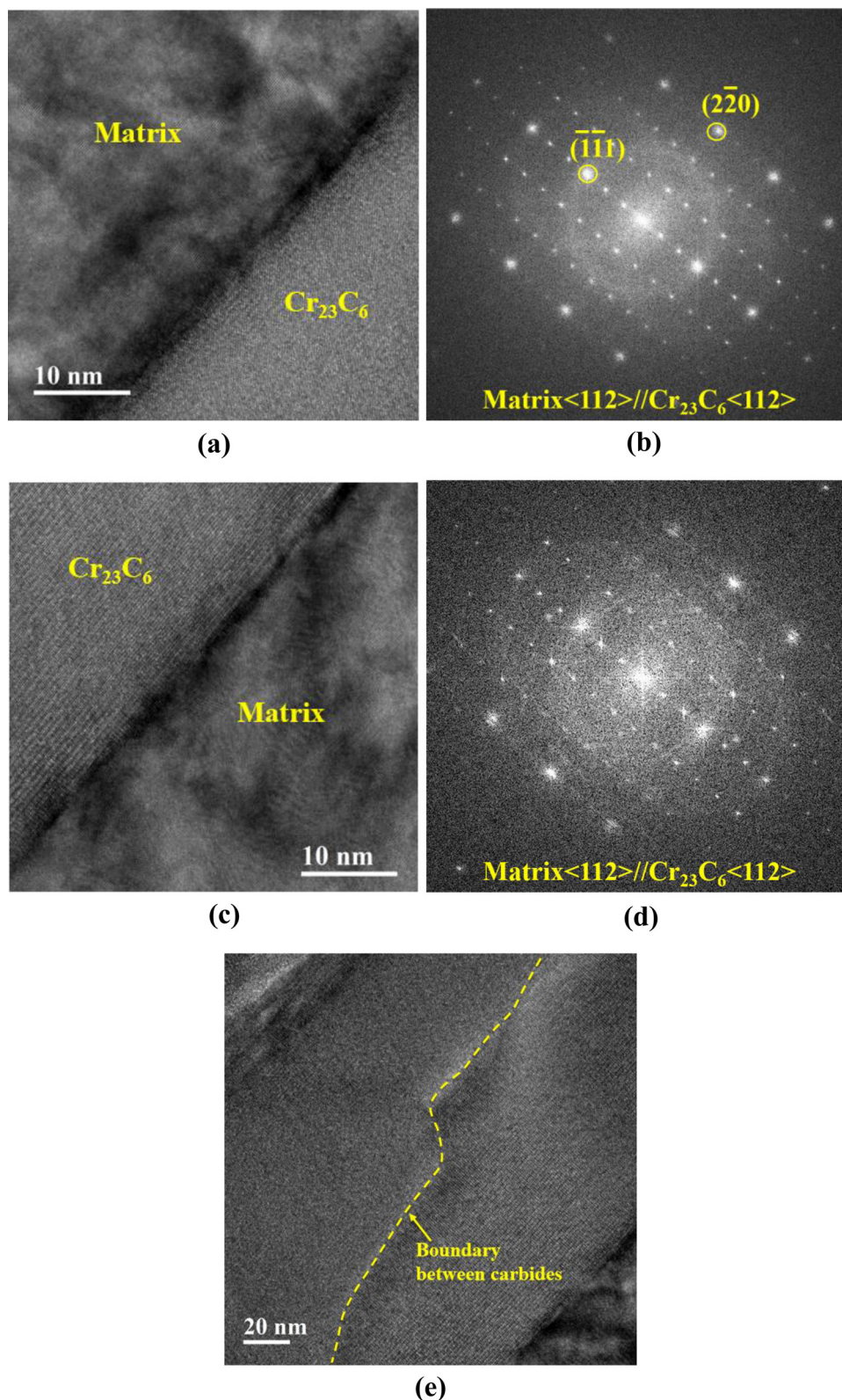


**Fig. 3.** (a), (c) High resolution TEM images of the carbide/matrix interfaces and (b), (d) the corresponding FFTs; (e) high resolution TEM image of the boundary between carbides.

Figs. 4 b-e show the EDS profiles along the corresponding lines in Fig. 4a. For the uncracked interface, line profile b indicates that the oxide is basically composed of Cr and O (Fig. 4b), confirming that the hematite structure is chromia. It should be noted that the carbide still contains some Ni (less than 10%). There is a transition layer in the

carbide which is enriched in Ni and depleted in Cr near the carbide/chromia interface, consistent with previous works on both alloy 690 [47] and alloy 600 [23,46,50]. The depletion of Cr in carbide can be easily blurred by the signal from chromia. Nevertheless, the depletion of Cr relative to the bulk carbide is still evident from the point where O

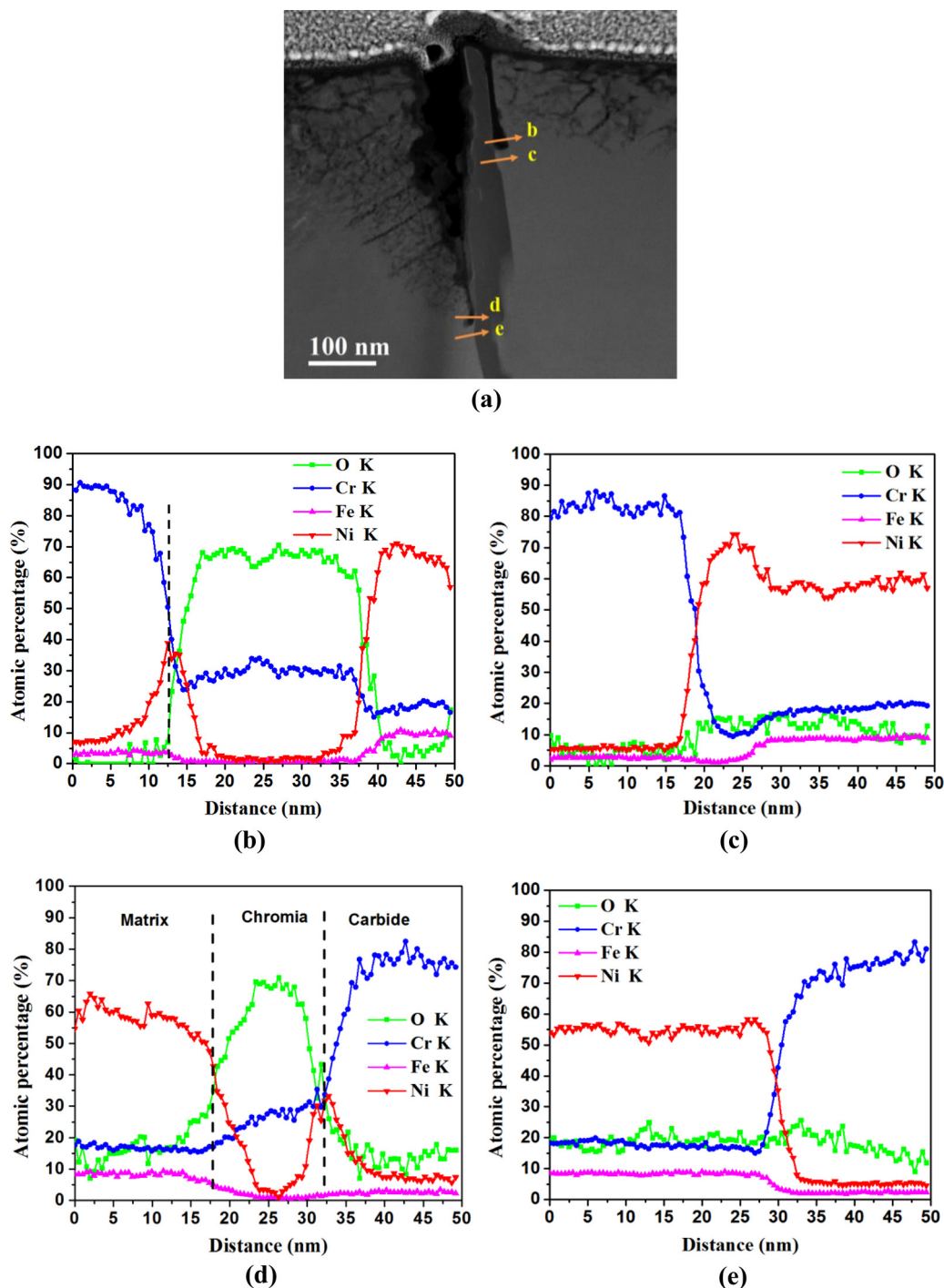
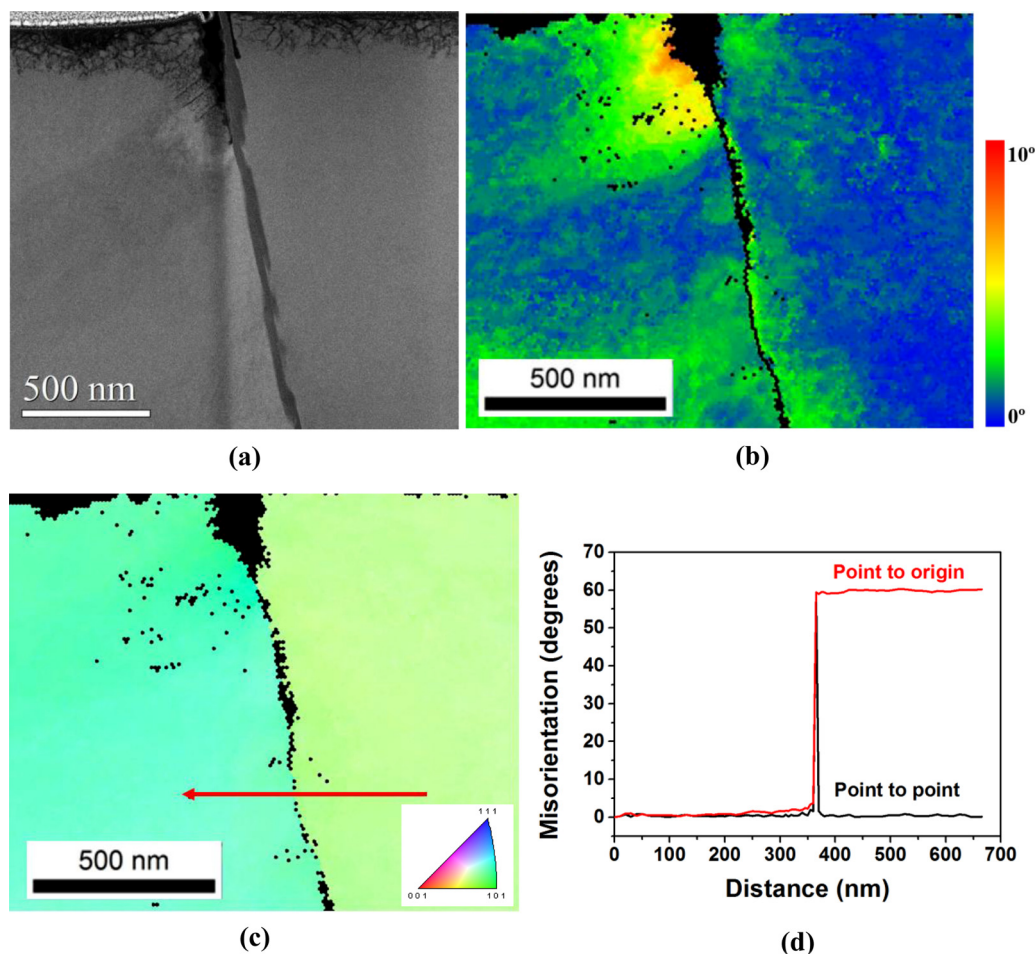


Fig. 4. (a) HAADF image of the cross section of sampled grain boundary and (b-e) EDS line profiles along the corresponding lines in (a).

decreases to the background level (denoted by the black dashed line in Fig. 4b). Meanwhile, no obvious Ni enrichment or Cr depletion is observed in the alloy near the chromia/matrix interface. It seems that Cr in chromia is mainly from the carbide. Beyond the chromia segment, the matrix shows a little Ni enrichment and Cr depletion near the carbide/matrix interface (Fig. 4c). For the cracked interface, the chromia segment beyond the crack is thinner than that formed along the uncracked interface. The boundaries of chromia were denoted with black broken lines at half of the maximum oxygen concentration in line profile d (Fig. 4d). It also shows Cr depletion and Ni enrichment on the carbide side near the chromia/carbide interface and insignificant composition change on the matrix side. Beyond the chromia, there is no

Cr depletion on the matrix side near the phase boundary (Fig. 4e), as opposed to line profile c.

The HAADF image of the FIB sample and the corresponding orientation deviation map are presented in Fig. 5 to evaluate the distribution of residual strain near the crack. Grain average orientation was used as the reference for each individual grain. The magnitude of orientation deviation from the reference reflects the level of residual strain. As only the residual strain in matrix is concerned here, the experiment condition for TKD measurement was optimized to improve the quality of diffraction patterns from the grain matrix while the patterns from carbide and oxide were poor and not indexable. The unindexable points are shown as black dots in Fig. 5b. The peak in orientation



**Fig. 5.** (a) HADDF image of the cross section of sampled grain boundary, (b) the corresponding orientation deviation (with reference to the grain average orientation) map and (c) inverse pole figure, and (d) misorientation profiles along the red arrow in (c).

deviation lies in the matrix adjacent to the cracked matrix/carbide interface and the deviation magnitude diminishes gradually as it moves away from the crack (Fig. 5b), indicating that plastic deformation concentrates around the crack. In contrast, the orientation deviation near the uncracked matrix/carbide interface is insignificant compared to the matrix background level, suggesting that there is no concentrated residual strain along the interface. Fig. 5c shows the inverse pole figure and Fig. 5d shows the misorientation profiles along the red arrow in Fig. 5c. The point to origin misorientation profile clearly indicates that the misorientation angle between these two grains is around 60 degrees.

#### 4. Discussion

This work studied a peculiar grain boundary which contains two matrix/carbide interfaces. The microstructures of crack and oxide formed along the matrix/carbide interface will first be analyzed. The oxidation kinetics will then be compared between the cracked and uncracked interfaces and the acceleration effects of stress concentration and deformation localization on oxidation will be discussed.

##### 4.1. Oxidation along the matrix/carbide interface

The sampled grain boundary shows a peculiar structure as a continuous intergranular carbide layer formed (Fig. 2a). The  $\langle 112 \rangle$  zone axes of these two grains coincide (Figs. 3b and 3d) and the misorientation between them is around 60 degrees (Fig. 5d), suggesting that the original grain boundary was a twin boundary. The carbide

layer is composed of two sub layers which are epitaxial with the neighboring grain matrixes and the interfaces are aligned with the  $\{111\}$  planes (Fig. 3). Thus, the boundary between these two sub carbide layers should inherit the original twin boundary structure and these two matrix/carbide interfaces have identical structure and should not cause any difference in oxidation kinetics. The crack initiation along one of the carbide/matrix interfaces is probably related to the blocking of dislocation transfer across the continuous carbide layer. The difference in susceptibility to crack initiation between these two interfaces probably results from the slight difference in Taylor factor between the grain matrixes. From the TKD measurement, the Taylor factor of the left grain (3.40) in Fig. 2b is lower than that of the right grain (3.52). So plastic deformation in the left grain is easier and leads to higher dislocation density, thus promoting the cracking process. Both interfaces are subject to penetrative oxidation. The formed chromia maintains specific orientation relationship with matrix (chromia  $\langle 100 \rangle //$  matrix  $\langle 112 \rangle$ , chromia  $\{006\} //$  matrix  $\{111\}$ ). Equivalent orientation relationship has also been found between chromia filaments and alloy 690 matrix [28,45]. It has also been reported that the chromia filaments form preferentially along the widely-spaced lattice planes of the matrix as the relatively wider lattice spacing allows easier diffusion of oxygen [45]. Thus, the preferential oxidation along the carbide/matrix interfaces should be partly due to the fact that the interface plane is  $\{111\}$  (Fig. 2). The higher oxide density into the matrix near the cracked carbide/matrix interface compared to that near the other uncracked interface (Fig. 5a) is probably related to the higher local dislocation density which is revealed in the orientation deviation map (Fig. 5b). The chromia layer along the uncracked matrix/carbide

interface is deeper than those internal oxide filaments formed in the matrix (Fig. 2b), suggesting that the carbide can promote the formation of chromia. Another supporting evidence is that the outer layer of carbide adjacent to the oxide is depleted in Cr and enriched in Ni (Figs. 4b and d). Thus, the carbide provides Cr for the chromia formation along the matrix/carbide interface, as suggested in some previous works [23,46]. In contrast, there is no significant Cr depletion in the matrix near the chromia layer (Figs. 4b and d), indicating that the lattice diffusion of Cr from the matrix is very limited, even in the highly deformed area near the crack (Fig. 5b). Consistent result has also been reported in a previous work [28]. It is worth mention that the local thermodynamic condition near the crack tip in hydrogenated water should not be significantly changed compared to the bulk solution as dissolved hydrogen diffuses fast enough [51]. The negligible variation in thermodynamic condition is also revealed from the fact that chromia oxide formed both beyond the crack and along the uncracked interface.

Beyond the oxide segment, there is a Cr-depleted zone in the matrix near the uncracked matrix/carbide interface (Fig. 4c) while no apparent Cr depletion was observed for the cracked one (Fig. 4e). The Cr depletion along the uncracked matrix/carbide interface could not be caused by carbide precipitation as both carbides formed under the same thermal treatment condition. Moreover, the EDS map of Cr (not provided here) shows that the Cr-depleted zone only extends several tens of nm beyond the oxide, confirming the Cr depletion only occurred during the oxidation stage. It should result from the formation of chromia along the interface which consumes the available Cr source nearby and results in the outward diffusion of Cr. Such Cr depletion didn't occur along the cracked matrix/carbide interface probably because the ingress of oxygen is much faster and oxygen can react with Cr from the adjacent carbide before extra Cr can timely diffuse to the oxidation front from the intact interface. Therefore, in this case, the controlling process for crack propagation should be oxygen diffusion, not Cr diffusion as suggested by Sennour et al. [23] and Guerre et al. [32].

#### 4.2. Acceleration in oxidation kinetics

The oxidation kinetics along both interfaces should be similar before crack initiation as they have the same structure, as indicated in Fig. 6a. It is reasonable to use parabolic law to describe the kinetics of oxidation along the interface since it is mainly controlled by oxygen diffusion:

$$L = k_p \cdot t^{1/2} \quad (1)$$

Here,  $L$  is the oxidation depth (in nm),  $t$  is the oxidation time (in h) and  $k_p$  is the rate constant. The crack initiates along one interface once the oxidation reaches a critical depth (Fig. 6b). Given that SCC crack grows smoothly on this alloy [52], it is assumed here that the crack propagates in a continuous mode and at the same rate as the oxide develops ahead of the crack, while oxidation proceeds following the same parabolic law for the uncracked interface. Thus, the depth of remaining oxide along the cracked interface is constant during crack propagation. From the measured oxidation depth along the uncracked interface (203.4 nm) and the total oxidation time (502 h),  $k_p$  is calculated to be  $9.08 \text{ nm} \cdot \text{h}^{-1/2}$ . From the remaining oxidation depth ahead of crack (175.1 nm) and  $k_p$ , crack initiation is calculated to occur at 372 h. Then the average crack growth rate, which equals oxidation rate ahead of the growing crack, is estimated to be  $2.935 \text{ nm/h}$  (i.e.  $8.15 \times 10^{-10} \text{ mm/s}$ ). This is a reasonable crack growth rate (CGR) for alloy 690 when compared with the data from CGR test on non-cold worked samples in simulated PWR primary water [52]. Meanwhile, the oxidation depth along the uncracked interface increased from 175.1 to 203.4 nm after crack initiation (as denoted by the red segment in Fig. 6c).

Fig. 7 shows the evolution of oxidation depth versus time. The black curve is the oxidation depth along the uncracked interface following parabolic law. At 372 h, crack initiates and the red solid line denotes the evolution of crack depth. The total crack depth  $L_o$  equals the increment in oxidation depth after crack initiation given that the crack is converted from oxide.  $L_o$  is the virtual increment in crack depth if the

oxidation kinetic was not affected by crack formation. The instant oxidation rate prior to crack initiation is the slope of the parabolic curve at 372 h, i.e.  $0.235 \text{ nm/h}$ .  $\Delta L$  is the increment in oxidation depth along the uncracked interface which is close to  $L_o$ . It should be mentioned that the stress state at the uncracked interface should alleviate a little after crack initiated at the other interface and affect the oxidation kinetics. However, it only occurs for the last 130 h when the oxidation rate is already quite low (Fig. 7) and would not change the overall parabolic law constant significantly. Thus, it is reasonable to assume that oxidation along the uncracked interface follows a single parabolic law. The ratio between  $L_o$  and  $L_o$  (i.e. 12.5) reflects a significant acceleration in oxidation kinetics due to cracking.

#### 4.3. Acceleration mechanism in oxidation kinetics

The acceleration factor (ratio between  $L_o$  and  $L_o$ ) is calculated from measured oxidation depths along two interfaces with identical structure. The major difference between these two interfaces is the existence of stress concentration and deformation localization near the cracked interface. Therefore, the acquired factor should reliably capture the acceleration effect of stress concentration or deformation localization or both on oxidation kinetics. The deformation localization near the cracked interface (Fig. 5b) should induce high dislocation density and accelerate the diffusivity in matrix [53,54] as the dislocation core is a fast diffusion path [55]. However, the high density of dislocation ahead of the crack probably has limited effect on the diffusion along the interface as the dislocation lines are unlikely to be aligned with the interface. The acceleration in oxidation kinetic should be related to other factors.

The oxidation kinetics is directly related to the flux of oxygen to the reaction front which depends on the concentration gradient of oxygen vacancy and diffusivity of oxygen. In the SAGBO model proposed by Evans et al. [39] and Ramsay et al. [40], the local stress  $\sigma$  affects the concentration of oxygen vacancy  $C_v$ , according to:

$$C_v = C_o \exp(\sigma \Omega_A / (kT)) \quad (2)$$

where  $C_o$  is the equilibrium vacancy concentration in the absence of stress,  $\Omega_A$  is the volume change resulting from oxidation,  $k$  is Boltzmann's constant and  $T$  is temperature in kelvin. Assuming the oxygen diffusivity is constant, the SAGBO parameter  $S_r$ , i.e. the ratio of oxide growth rate between stressed and unstressed condition, is formulated as [39,40]:

$$S_r = \exp(\sigma_{ap} \Omega_A / (kT)) \quad (3)$$

where  $\sigma_{ap}$  is the applied stress at the tip of oxide intrusion. In this work, the depth of oxide intrusion ahead of crack tip and the crack growth rate are assumed constant, so the ratio of oxide growth rate equals that of virtual increment in oxide depth. It should be noted that the local stress at the oxide tip changes as the crack propagates. To estimate the upper limit of the SAGBO parameter, the final applied stress ( $\sim 300 \text{ MPa}$ ) and crack size (length:  $\sim 10 \mu\text{m}$ , depth:  $381.5 \text{ nm}$ ) are used to estimate the local tensile stress at oxide tip. Assuming the surface crack is elliptical as measured on alloy 600 [56], the stress intensity factor is estimated according to the finite element analysis from Shin and Cai [57] which shows that the geometry correction factor is not very sensitive to the size of very shallow crack. The local applied stress at the oxide tip (175.1 nm from the crack tip) is calculated to be around  $330 \text{ MPa}$ . As we are comparing the oxidation kinetics at different applied stress states here, the difference in stress (i.e.  $30 \text{ MPa}$ ) instead of  $\sigma_{ap}$  should be used in equation (3).  $\Omega_A$  ( $\Omega_{\text{Cr}_2\text{O}_3-2/23\Omega_{\text{Cr}_23\text{C}_6}}$ ) is calculated to be  $2.24 \times 10^{-29} \text{ m}^3$  for the formation of chromia from  $\text{Cr}_{23}\text{C}_6$ . Thus, an upper limit of SAGBO parameter, i.e. 1.08, is acquired from equation (3), which is much smaller than the ratio between  $L_o$  and  $L_o$  mentioned above (i.e. 12.5). Apparently, the stress concentration induced by such a tiny crack is too small to cause much effect on the oxidation kinetics. The SAGBO model proposed by Evans and Ramsay could not explain the acceleration in oxidation kinetics ahead of crack tip.

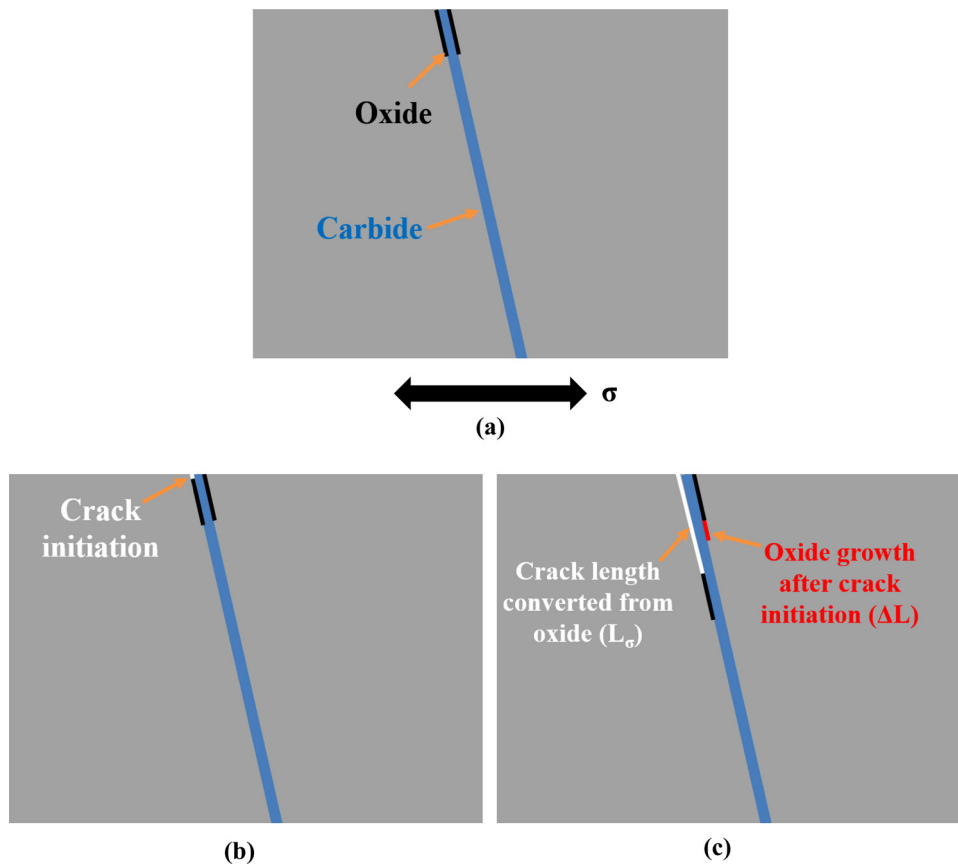


Fig. 6. Schematic showing the evolution of cracking and oxidation along the matrix/carbide interfaces ((a) prior to crack initiation, (b) crack initiation and (c) after crack initiation).

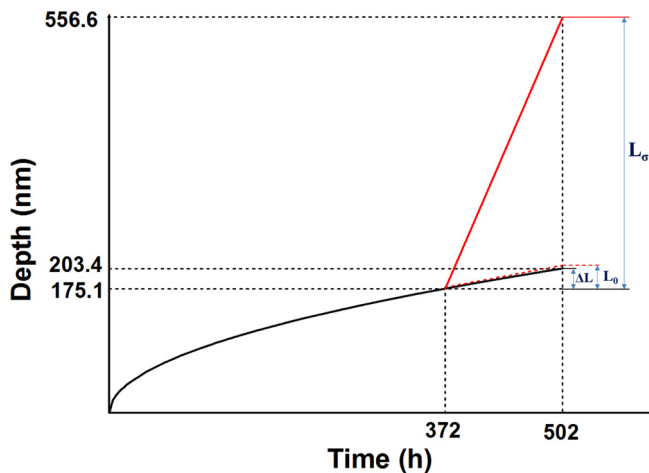


Fig. 7. Evolution of oxidation depth under different situations ( $\Delta L$ - the increment in oxidation depth along the uncracked interface,  $L_{\sigma}$ -the virtual increment in oxidation depth when the oxidation kinetic was not affected,  $L_{\sigma}$ -the increment in oxidation depth after crack initiation which equals the crack depth).

It should be noted that the diffusivity of oxygen was held constant in the model proposed by Evans et al. [39] and Ramsay et al. [40]. However, increasing evidences suggest that high vacancy concentration induced by plastic deformation can greatly accelerate the diffusivities of atoms and even promote phase transformation or precipitation [58–60]. The diffusivity of oxygen should also be enhanced by high vacancy concentration near the crack which results from the localization of plastic deformation (as revealed in Fig. 5). Arioka et al. [61] recently reported that excess vacancies could migrate to the highly

stressed region near a notch center and notably promote the diffusivity of Ni in 20% cold-worked 316 stainless steel. Their measurement shows that the diffusion coefficient of Ni at a tensile stress of 553 MPa is 6.5 times higher than that at the low-stress zone at 450 °C [61]. In this work, carbide can serve as a convenient Cr source for the formation of chromia as Cr depletion is mainly on the carbide side (Figs. 4b and 4d). Thus, oxygen diffusion is the controlling process in the penetrative oxidation along the carbide/matrix interface. If the change in diffusivity of oxygen vacancy was considered, equation (3) can be revised as:

$$S_r = L_{\sigma}/L_0 = (D_{\sigma}/D_0) \cdot \exp(\sigma_{ap} \cdot \Omega_A / (kT)) \quad (4)$$

where  $D_{\sigma}$  and  $D_0$  are the diffusion coefficients of oxygen vacancy under stressed and unstressed situations.  $D_{\sigma}/D_0$  should be 11.57 to achieve a  $S_r$  of 12.5. So the diffusion coefficient of oxygen vacancy ahead of the growing crack is over an order of magnitude faster than that when there is no crack. Compared with stress concentration, deformation localization plays a dominant role in accelerating the oxidation kinetics.

The above analysis clearly indicates that deformation localization ahead of crack tip can greatly accelerate the transportation of oxygen to the reaction front. Given that intergranular oxidation is an indispensable precursor in the SCC process of the Fe-Cr-Ni alloys in high temperature water, the CGR should be directly related to the oxidation kinetics ahead of the growing crack. Accordingly, it is feasible to predict CGR by formulating the oxidation kinetics with the acceleration in oxygen transportation being fully addressed. It may be a promising pathway to model the propagation of SCC.

## 5. Conclusion

A peculiar grain boundary sampled from alloy 690 was studied after constant extension rate tensile (CERT) test in simulated PWR primary

water. The grain boundary contains two identical matrix/carbide interfaces, one of which cracked due to lower resistance to deformation in the adjacent matrix. Oxide formed ahead of the crack with no apparent diffusion of Cr from the surrounding matrix, suggesting that oxidation, a precursor for crack propagation, is mainly controlled by oxygen diffusion. Both interfaces formed a segment of compact chromia from the exposed end but at different rates.

The kinetics study indicates that the oxidation rate ahead of the growing crack was promoted by over an order of magnitude compared to that when the interface is intact. Stress concentration ahead of the crack tip only slightly increased the oxidation rate while the deformation localization plays a dominant role in accelerating oxidation kinetics as the associated high vacancy concentration can promote the diffusivity of oxygen by over an order of magnitude.

#### Data availability

The raw/processed data required to reproduce these findings cannot be shared at this time as the data also forms part of an ongoing study.

#### CRediT authorship contribution statement

**Wenjun Kuang:** Conceptualization, Data curation, Funding acquisition, Investigation, Supervision, Writing-review & editing. **Miao Song:** Methodology, Data curation. **Xingyu Feng:** Methodology, Data curation.

#### Declaration of Competing Interest

There is no conflict of interest.

#### Acknowledgements

The authors gratefully acknowledge the financial support of National Natural Science Foundation of China (No. 51971172), the Fundamental Research Funds for the Central Universities (xjh012019005) and the Young Talent Support Plan of Xi'an Jiaotong University. The authors would like to thank Dr. Chao Li at Instrument Analysis Center of Xi'an Jiaotong University for his assistance in STEM and EDS analysis and Dr. Donghai Du from University of Michigan for helping with the EBSD analysis.

#### Appendix A. Supplementary data

Supplementary material related to this article can be found, in the online version, at doi:<https://doi.org/10.1016/j.corsci.2020.108943>.

#### References

- [1] P.M. Scott, P. Combrade, Corrosion in Pressurized Water Reactor, ASM Handbook 13C ASM International, 2006.
- [2] S.J. Zinkle, G.S. Was, Materials challenges in nuclear energy, *Acta Mater.* 61 (2013) 735–758.
- [3] R.W. Staehle, Historical views on stress corrosion cracking of nickel-based alloys: The Coriou effect, *Stress Corrosion Cracking of Nickel Based Alloys in Water-cooled Nuclear Reactors*, Woodhead Publishing, 2016.
- [4] P.M. Scott, M.L. Calvar, Some possible mechanisms of intergranular stress corrosion cracking of alloy 600 in PWR primary water, Sixth international symposium on environmental degradation of materials in nuclear power systems- water reactors, (1993) San Diego, Ca, USA.
- [5] R.C. Newman, T.S. Gendron, P.M. Scott, Internal oxidation and embrittlement of alloy 600, Ninth international symposium on environmental degradation of materials in nuclear power systems- water reactors, Newport Beach, Ca, USA, (1999).
- [6] P.M. Scott, An overview of internal oxidation as a possible explanation of intergranular stress corrosion cracking of alloy 600 in PWRs, Ninth international symposium on environmental degradation of materials in nuclear power systems- water reactors, (1999) Newport Beach, Ca, USA.
- [7] M.B. Capell, S.G. Was, Selective Internal Oxidation as a Mechanism for Intergranular Stress Corrosion Cracking of Ni-Cr-Fe Alloys, *Metall. Mater. Trans. A* 38 (2007) 1244–1259.
- [8] P.M. Scott, P. Combrade, General corrosion and stress corrosion cracking of Alloy 600 in light water reactor primary coolants, *J. Nucl. Mater.* 524 (2019) 340–375.
- [9] K. Fujii, T. Miura, H. Nishioka, K. Fukuya, Degradation of grain boundary strength by oxidation in alloy 600, 15th Int. Conf. on Environmental Degradation of Materials in Nuclear Power Systems-water reactors, Colorado Springs, Colorado, USA, 2011.
- [10] H. Dugdale, D.E.J. Armstrong, E. Tarleton, S.G. Roberts, S. Lozano-Perez, How oxidized grain boundaries fail, *Acta Mater.* 61 (2013) 4707–4713.
- [11] J. Dohr, E. Tarleton, D. Armstrong, T. Couvant, S. Lozano-Perez, Recent insights in the deformation and fracture of oxidized grain boundaries in austenitic alloys: a synergistic experimental and finite element study, 17th Int. Conf. on Environmental Degradation of Materials in Nuclear Power Systems-water reactors, Ottawa, Ontario, Canada, 2015.
- [12] A. Stratulat, D.E.J. Armstrong, S.G. Roberts, Micro-mechanical measurement of fracture behaviour of individual grain boundaries in Ni alloy 600 exposed to a pressurized water reactor environment, *Corros. Sci.* 104 (2016) 9–16.
- [13] M.J. Olszta, D.K. Schreiber, M.B. Toloczko, S.M. Brummer, Alloy 690 surface nanostructures during exposure to PWR primary water and potential influence on stress corrosion crack initiation, The 16th international conference on environmental degradation of materials in nuclear power systems-water reactors, Asheville, North Carolina, USA, 2013.
- [14] T. Moss, G. Cao, G.S. Was, Oxidation of Alloy 600 and Alloy 690: Experimentally Accelerated Study in Hydrogenated Supercritical Water, *Metall. Mater. Trans. A* (2017) 1–17.
- [15] W. Kuang, G.S. Was, The effect of grain boundary structure on the intergranular degradation behavior of solution annealed alloy 690 in high temperature, hydrogenated water, *Acta Mater.* 182 (2020) 120–130.
- [16] T. Moss, W. Kuang, G.S. Was, Stress corrosion crack initiation in Alloy 690 in high temperature water, *Curr. Opin. Solid State Mater. Sci.* 22 (2018) 16–25.
- [17] W. Kuang, G.S. Was, A high-resolution characterization of the initiation of stress corrosion crack in Alloy 690 in simulated pressurized water reactor primary water, *Corros. Sci.* 163 (2020) 108243.
- [18] T. Terachi, K. Fujii, K. Arioka, Microstructural Characterization of SCC Crack Tip and Oxide Film for SUS 316 Stainless Steel in Simulated PWR Primary Water at 320°C, *J. Nucl. Sci. Technol.* 42 (2005) 225–232.
- [19] M. Meisnar, M. Moody, S. Lozano-Perez, Atom probe tomography of stress corrosion crack tips in SUS316 stainless steels, *Corros. Sci.* 98 (2015) 661–671.
- [20] Y.H. Lu, Q.J. Peng, T. Sato, T. Shoji, An ATEM study of oxidation behavior of SCC crack tips in 304L stainless steel in high temperature oxygenated water, *J. Nucl. Mater.* 347 (2005) 52–68.
- [21] Z. Shen, D. Du, L. Zhang, S. Lozano-Perez, An insight into PWR primary water SCC mechanisms by comparing surface and crack oxidation, *Corros. Sci.* 148 (2019) 213–227.
- [22] L.E. Thomas, S.M. Brummer, High-Resolution Characterization of Intergranular Attack and Stress Corrosion Cracking of Alloy 600 in High-Temperature Primary Water, *Corrosion* 56 (2000) 572–587.
- [23] M. Sennour, P. Laghoutaris, C. Guerre, R. Molins, Advanced TEM characterization of stress corrosion cracking of Alloy 600 in pressurized water reactor primary water environment, *J. Nucl. Mater.* 393 (2009) 254–266.
- [24] Y.S. Lim, H.P. Kim, S.S. Hwang, Microstructural characterization on intergranular stress corrosion cracking of Alloy 600 in PWR primary water environment, *J. Nucl. Mater.* 440 (2013) 46–54.
- [25] Z. Shen, K. Arioka, S. Lozano-Perez, A mechanistic study of SCC in Alloy 600 through high-resolution characterization, *Corros. Sci.* 132 (2018) 244–259.
- [26] S. Lozano-Perez, J.M. Titchmarsh, TEM investigations of intergranular stress corrosion cracking in austenitic alloys in PWR environmental conditions, *Mater. High Temp.* 20 (2003) 573–579.
- [27] T. Moss, G.S. Was, Accelerated Stress Corrosion Crack Initiation of Alloys 600 and 690 in Hydrogenated Supercritical Water, *Metall. Mater. Trans. A* 48 (2017) 1613–1628.
- [28] W. Kuang, M. Song, G.S. Was, Insights into the stress corrosion cracking of solution annealed alloy 690 in simulated pressurized water reactor primary water under dynamic straining, *Acta Mater.* 151 (2018) 321–333.
- [29] R.W. Staehle, Z. Fang, Comments on a proposed mechanism of internal oxidation for alloy 600 as applied to low potential SCC, Proceedings of 9th International Symposium on Environmental Degradation of Materials in Nuclear Power Systems-Water Reactors, Newport Beach, CA, USA, 1999.
- [30] E.P. Simonen, L.E. Thomas, S.M. Brummer, Diffusion Kinetic Issues During Intergranular Corrosion of Ni-Base Alloys, *Corrosion* 2000, NACE International, 2000.
- [31] S. Lozano-Perez, T. Yamada, T. Terachi, M. Schroder, C.A. English, G.D.W. Smith, C.R.M. Grovonor, B.L. Eyre, Multi-scale characterization of stress corrosion cracking of cold-worked stainless steels and the influence of Cr content, *Acta Mater.* 57 (2009) 5361–5381.
- [32] C. Guerre, P. Laghoutaris, J. Chene, L. Marchetti, R. Molins, C. Duhamel, M. Sennour, Stress corrosion cracking of alloy 600 in PWR primary water: influence of chromium, hydrogen and oxygen diffusion, 15th Int. Conf. on Environmental Degradation of Materials in Nuclear Power Systems-water reactors, Colorado Springs, Colorado, USA, 2011.
- [33] E. Andrieu, R. Molins, H. Ghonem, A. Pineau, Intergranular crack tip oxidation mechanism in a nickel-based superalloy, *Mater. Sci. Eng. A* 154 (1992) 21–28.
- [34] L. Viskari, M. Hörnqvist, K.L. Moore, Y. Cao, K. Stiller, Intergranular crack tip oxidation in a Ni-base superalloy, *Acta Mater.* 61 (2013) 3630–3639.
- [35] H.S. Kitaguchi, H.Y. Li, H.E. Evans, R.G. Ding, L.P. Jones, G. Baxter, P. Bowen, Oxidation ahead of a crack tip in an advanced Ni-based superalloy, *Acta Mater.* 61 (2013) 1968–1981.

- [36] H.S. Kitaguchi, M.P. Moody, H.Y. Li, H.E. Evans, M.C. Hardy, S. Lozano-Perez, An atom probe tomography study of the oxide-metal interface of an oxide intrusion ahead of a crack in a polycrystalline Ni-based superalloy, *Scripta Mater.* 97 (2015) 41–44.
- [37] A.A.N. Németh, D.J. Crudden, D.E.J. Armstrong, D.M. Collins, K. Li, A.J. Wilkinson, C.R.M. Grovenor, R.C. Reed, Environmentally-assisted grain boundary attack as a mechanism of embrittlement in a nickel-based superalloy, *Acta Mater.* 126 (2017) 361–371.
- [38] D.F. Smith, E.F. Clatworthy, D.G. Tipton, W.L. Mankins, Improving the notch-rupture strength of low-expansion superalloys, *Proc. 4th Int. Conf. on Superalloys*, Seven Springs, Pa, 1980.
- [39] H.E. Evans, H.Y. Li, P. Bowen, A mechanism for stress-aided grain boundary oxidation ahead of cracks, *Scripta Mater.* 69 (2013) 179–182.
- [40] J.D. Ramsay, H.E. Evans, D.J. Child, M.P. Taylor, M.C. Hardy, The influence of stress on the oxidation of a Ni-based superalloy, *Corros. Sci.* 154 (2019) 277–285.
- [41] T. Shoji, Z. Lu, The effect of strain-hardening on PWSCC of nickel-base alloys 600 and 690, 14th international conference on environmental degradation of materials in nuclear power systems, Virginia Beach, VA, 2009.
- [42] W. Kuang, G.S. Was, The effects of grain boundary carbide density and strain rate on the stress corrosion cracking behavior of cold rolled Alloy 690, *Corros. Sci.* 97 (2015) 107–114.
- [43] W. Kuang, G.S. Was, The effects of strain rate and carbon concentration on the dynamic strain aging of cold rolled Ni-based alloy in high temperature water, *Scripta Mater.* 107 (2015) 107–110.
- [44] W. Kuang, G.S. Was, C. Miller, M. Kaufman, T. Alam, B. Gwalani, R. Banerjee, The effect of cold rolling on grain boundary structure and stress corrosion cracking susceptibility of twins in alloy 690 in simulated PWR primary water environment, *Corros. Sci.* 130 (2018) 126–137.
- [45] W. Kuang, M. Song, P. Wang, G.S. Was, The oxidation of alloy 690 in simulated pressurized water reactor primary water, *Corros. Sci.* 126 (2017) 227–237.
- [46] S.M. Bruemmer, L.E. Thomas, High-resolution analytical electron microscopy characterization of corrosion and cracking at buried interfaces, *Surf. Interface Anal.* 31 (2001) 571–581.
- [47] M.J. Olszta, D.K. Schreiber, L.E. Thomas, S.M. Bruemmer, Penetrative internal oxidation from alloy 690 surface and stress corrosion crack walls during exposure to PWR primary water, 15th Int. Conf. on Environmental Degradation of Materials in Nuclear Power Systems-water reactors, Colorado Springs, Colorado, USA, 2011.
- [48] H. Li, S. Xia, B. Zhou, W. Chen, C. Hu, The dependence of carbide morphology on grain boundary character in the highly twinned Alloy 690, *J. Nucl. Mater.* 399 (2010) 108–113.
- [49] Y.S. Lim, D.J. Kim, S.S. Hwang, H.P. Kim, S.W. Kim, M23C6 precipitation behavior and grain boundary serration in Ni-based Alloy 690, *Mater. Charact.* 96 (2014) 28–39.
- [50] Y.S. Lim, S.W. Kim, S.S. Hwang, H.P. Kim, C. Jang, Intergranular oxidation of Ni-based Alloy 600 in a simulated PWR primary water environment, *Corros. Sci.* 108 (2016) 125–133.
- [51] W. Kuang, J. Hesterberg, G.S. Was, The effect of post-irradiation annealing on the stress corrosion crack growth rate of neutron-irradiated 304L stainless steel in boiling water reactor environment, *Corros. Sci.* 161 (2019) 108183.
- [52] M.B. Toloczko, S.M. Bruemmer, Crack growth response of Alloy 690 in simulated PWR primary water, 14th Int. Conf. on Environmental Degradation of Materials in Nuclear Power Systems, Virginia Beach, VA, 2009.
- [53] E.W. Hart, On the role of dislocations in bulk diffusion, *Acta Metall.* 5 (1957) 597.
- [54] A.L. Ruoff, R.W. Balluffi, Strain-Enhanced Diffusion in Metals. II. Dislocation and Grain-Boundary Short-Circuiting Models, *J. Appl. Phys.* 34 (1963) 1848–1853.
- [55] M. Legros, G. Dehm, E. Arzt, T.J. Balk, Observation of Giant Diffusivity Along Dislocation Cores, *Science* 319 (2008) 1646.
- [56] Z. Zhai, M.B. Toloczko, M.J. Olszta, S.M. Bruemmer, Stress corrosion crack initiation of alloy 600 in PWR primary water, *Corros. Sci.* 123 (2017) 76–87.
- [57] C.S. Shin, C.Q. Cai, Experimental and finite element analyses on stress intensity factors of an elliptical surface crack in a circular shaft under tension and bending, *Int. J. Fract.* 129 (2004) 239–264.
- [58] B.B. Straumal, A.A. Mazilkin, B. Baretzky, uuml Sch, G. tz, E. Rabkin, R.Z. Valiev, Accelerated Diffusion and Phase Transformations in Co&ndash;Cu Alloys Driven by the Severe Plastic Deformation, *Mater. Trans.* 53 (2012) 63–71.
- [59] K. Arioka, Y. Iijima, T. Miyamoto, Rapid nickel diffusion in cold-worked type 316 austenitic steel at 360–500 °C, *Int. J. Mater. Res.* 108 (2017) 791–797.
- [60] W. Sun, Y. Zhu, R. Marceau, L. Wang, Q. Zhang, X. Gao, C. Hutchinson, Precipitation strengthening of aluminum alloys by room-temperature cyclic plasticity, *Science* 363 (2019) 972.
- [61] K. Arioka, Y. Iijima, M. Miyamoto, Acceleration of nickel diffusion by high tensile stress in cold-worked type 316 stainless steel at 450°C, *Philos. Mag.* (2018) 1–9.